IEEE Open Journal of Vehicular Technology

Received 27 July 2024; accepted 19 August 2024. Date of publication 26 August 2024;
date of current version 13 September 2024. The review of this article was coordinated by Editor Jianping He.

Digital Object Identifier 10.1109/OJVT.2024.3450279

Dynamic Full-Duplex Cellular System for Wide Area IoT Network Backbone

KEIICHI MIZUTANI (Member, IEEE), KAZUKI NISHIKORI, KYOYA TERAMAE, HIROTO KURIKI, TAKESHI MATSUMURA (Member, IEEE), AND HIROSHI HARADA (Senior Member, IEEE)

Graduate School of Informatics, Kyoto University, Kyoto 606-8501, Japan

CORRESPONDING AUTHOR: KEIICHI MIZUTANI (e-mail mizutani@i.kyoto-u.ac.jp).

This work was supported in part by MIC SCOPE under Grant175007004 and in part by the Ministry of Internal Affairs and Communications in Japan under Grant JPJ000254.

An earlier version of this paper was presented at the 21st International Symposium on Wireless Personal Multimedia Communications (WPMC), Chiang Rai, Thailand, Nov. 2018 [DOI: 10.1109/WPMC.2018.8713129.] and the IEEE 30th Annual International Symposium on Personal, Indoor and Mobile Radio Communications (PIMRC), Istanbul, Türkiye, Sep. 2019 [DOI: 10.1109/PIMRC.2019.8904172].

ABSTRACT This study proposes a dynamic full-duplex cellular (DDC) system by introducing an in-band full-duplex in a phased manner into a conventional time-division duplex (TDD)-based cellular system. Further, we propose and evaluate appropriate user equipment (UE) scheduling and transmission power control schemes for DDC in dense urban multi-cell environments. The proposed DDC sufficiently suppresses inter-cell interference through fully distributed resource allocation, which does not require information exchange among neighboring cells. In particular, the propagation loss compensation factor, UE transmission power limit, and assumed uplink signal-to-noise plus interference power ratio (SINR) adjustment factor prove to be essential. By appropriately setting these factors, the proposed DDC system improves the average throughput of the downlink (DL) by 13.2% and uplink by 31.6% compared with the conventional TDD system. Moreover, we observe a 2.5% improvement in the DL 5% user throughput. The results of this study are expected to contribute to the realization of a high-capacity wide-area IoT network backbone by improving the efficiency of utilization of limited spectral resources, especially in the sub-6 GHz band.

INDEX TERMS Cellular, dynamic-full-duplex cellular, in-band full-duplex, IoT, time-division duplex.

I. INTRODUCTION

The rapid development of the Internet of Things (IoT) is underway, connecting various objects to the Internet, and enabling the exchange of data and control processes. The number of IoT devices on the planet was 6.1 billion in 2018 and is expected to increase to 14.7 billion by 2023 [1]. These numerous IoT devices will be connected to the Internet via non-cellular systems on an unlicensed spectrum, cellular systems on a licensed spectrum, or both. The two types of cellular system-based IoT network topologies are shown in Fig. 1. An IoT network comprising the third-generation partnership project (3GPP)-specified systems for IoT (3GPP-IoT), such as narrow-band IoT (NB-IoT) [2], [3], [4] or enhanced machine-type communication (eMTC) / Long-Term Evolution (LTE)-MTC (LTE-M) [3], [4]. In this topology, mobile and location-fixed IoT devices equipped with the user equipment (UE) of the 3GPP-IoT communicate directly with cellular base stations (BSs). A secure IoT network can be built because all UEs can be managed by the core network. In addition, high-reliability communication can be achieved because communication is completed only in the licensed band. However, all IoT devices must be equipped with a UE contracted with a telecommunications carrier, thus increasing the operating cost.

An IoT network comprising cellular and non-cellular systems is shown in Fig. 1(b). An example of a typical non-cellular system for IoT network construction in an unlicensed spectrum is the smart wireless ubiquitous network (Wi-SUN) [5]. In Particular, Wi-SUN for field area network profile (Wi-SUN FAN) [6], [7], [8], [9], [10], [11] can construct a mesh network through multi-hop relaying, making it suitable for IoT network construction in urban areas with numerous

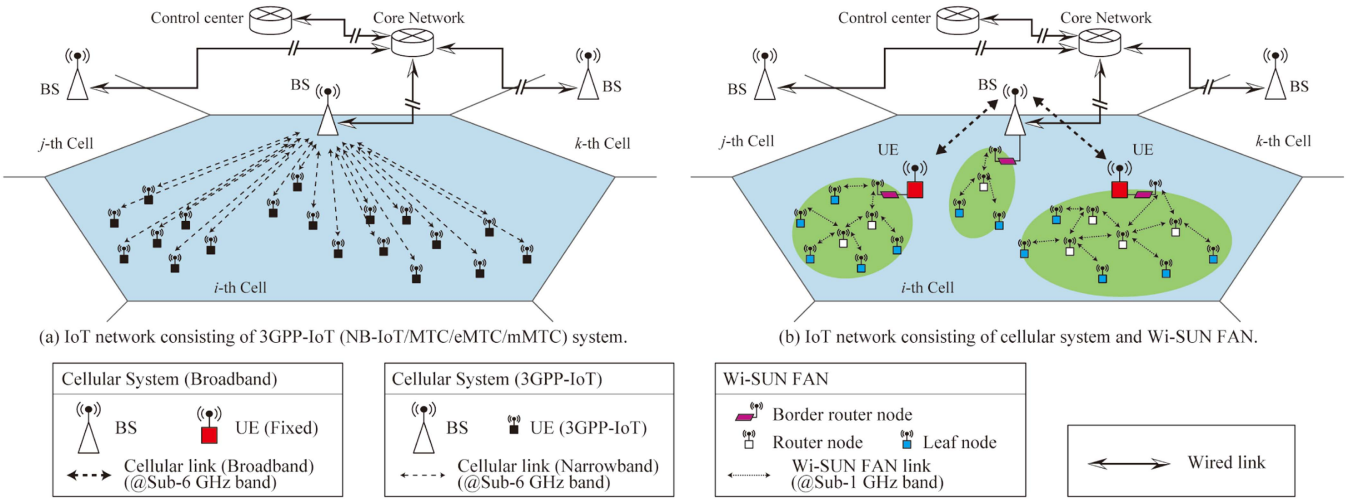

FIGURE 1. Cellular system-based IoT network topologies.

radio-quiet zones. In this topology, mobile and location-fixed IoT devices equipped with Wi-SUN FAN leaf or router nodes communicate with Wi-SUN FAN border router nodes through multi-hop relaying. The Wi-SUN FAN border router node is connected to the cellular UE (or BS) as shown in Fig. 1(b). Data collected by the Wi-SUN FAN are transported to the UE and transmitted to the BS via a cellular uplink (UL). Control signals to each IoT device are delivered through the Wi-SUN FAN after being sent from the BS to the UE over the cellular downlink (DL). This topology allows the required communication of massive IoT devices to be aggregated to a few locations by utilizing an unlicensed spectrum and minimizes the number of UEs contracted with telecommunications carriers, which is expected to reduce operating costs for IoT network operators. However, cellular communications require a large amount of aggregated IoT-related data to be transmitted in a limited frequency band; thus, improving the spectral efficiency of the communication between the BS and each UE is imperative.

To manage the increasing wireless communication traffic, improving the user data rate and spectral efficiency is a fundamental challenge for beyond-fifth-generation mobile communication systems. In addition to these requirements, the constant spectrum shortage in legacy frequency bands below 6 GHz (sub-6 GHz band) motivates the utilization of millimeter-wave and terahertz bands to significantly increase the data rate and communication capacity [12], [13]. However, an increase in the communication capacity in the sub-6 GHz band is essential for the sustainable and advanced utilization of the existing orthogonal frequency-division multiplexing (OFDM)-based cellular systems.

The in-band full-duplex (IBFD) [14], [15], [16], [17], [18], [19], [20], [21], [22], [23], [24], [25], [26], [27], [28], [29], [30], [31], [32], [33], [34], [35] is a promising technology for enhancing communication capacity. Because transmission and reception are simultaneously performed in the same frequency band in the IBFD system, the communication capacity

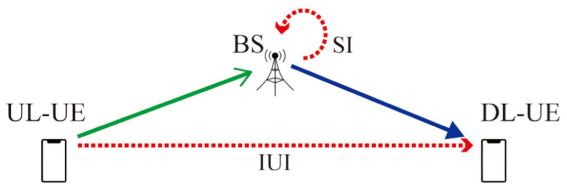

FIGURE 2. Basic architecture of the UP-IBFD system.

can be theoretically doubled compared with a conventional half-duplex (HD) system. In particular, a user-paired IBFD (UP-IBFD), as shown in Fig. 2 [17], [18], [19], [20], which simultaneously receives a UL signal from one UE and transmits a DL signal to another UE at the BS, is highly compatible with cellular systems (full-duplex cellular (FDC) systems) because no additional circuitry for IBFD is required at the UE. UP-IBFD is referred to as IBFD hereinafter. Self-interference (SI), a scenario in which the transmitted signal propagates in its own receiving circuit [16], [17], [18], [19], [20], [21], [22], [23], [24], [25], [26], [27], [28], [29], [30], [31], [32], [33], [34], and inter-UE interference (IUI), which is the interference caused by a UE transmitting a UL signal (UL-UE) to a UE receiving a DL signal (DL-UE) are major problems that must be overcome to realize an IBFD system [17], [18], [35]. The SI should be reduced and the IUI should be mitigated to accurately demodulate the desired signals. Many studies on SI cancellation methods, mainly in the antenna, analog, and digital domains have been reported. Moreover, the feasibility of achieving an SI cancellation performance of approximately 110 dB is increasing [16], [17], [18], [19], [20], [21], [22], [23], [24], [25], [26], [27], [28], [29], [30], [31], [32], [33], [34]. Assuming these SI cancellation performances can be realized in the BS, scheduling and power control algorithms for terminals implementing IBFD have been proposed [36], [37], [38], [39]. In these studies, theoretical formulas for UE scheduling that consider inter-UE fairness and the average sum rate have been proposed. However, these algorithms assume single cells [36], [37], [38] or multiple

cells but only apply IBFD to the central cell [39]. To the best of our knowledge, no practical algorithm that increases the IBFD application range to multiple cells and considers inter-cell interference (ICI) and IUI has been proposed. In addition, pursuing upper-bound values by utilizing theoretical formulas differs from the development of actual scheduling protocols and consideration of a feasible system throughput. Furthermore, a scheduling method that suddenly changes all current 5G systems is not feasible when the practical applications of FDC are considered. Therefore, a step-by-step method that considers backward compatibility and system performance evaluation is necessary.

This study proposes a dynamic full-duplex cellular (DDC) system to gradually extend the current HD-based cellular (HDC) system to an FDC system with the introduction of an IBFD communication. The proposed DDC system is based on a conventional HDC system, in which the DL or UL communication of another UE is superimposed by the IBFD only when the UL or DL communication of the UE already allocated by time-division duplex (TDD) is not influenced. This study proposes a scheduling method to select the UEs to apply to the IBFD, and a power control method to improve the quality of IBFD communication. We evaluate the performance of the proposed method through computer simulations as a DDC system based on an LTE-compliant system with a bandwidth of 20 MHz.

In previous versions of this study [14], [15], we proposed the basic concept of a DDC system, and the initial performance was evaluated in macro-cell [14] and dense urban microcell environments [15]. The average user throughput and lower 5% user throughput of the proposed DDC system were presented by utilizing link-level and system-level computer simulations [15]. This study is an extended version of [15], in which the technical background, system model, and algorithms of the proposed system are described and organized in more detail, and the UE energy efficiency and IBFD application ratio of the proposed system are further evaluated and discussed in addition to the results of [15]. In particular, the main contribution of this study is to show that the proposed DDC system has a higher throughput improvement rate than the UE energy efficiency degradation rate by evaluating and discussing both throughput and energy efficiency simultaneously.

The remainder of this paper is organized as follows. Section II explains the duplex schemes for cellular systems; Section III proposes the DDC system with the presentation of the interference models, proposed scheduling method, and proposed power control method. Section IV evaluates the proposed DDC system through computer simulations. Finally, Section V concludes the paper.

The variables, coefficients, and their definitions are listed in Table 1.

TABLE 1. Parameters and Their Definitions

Parameters	Definitions	Remarks
Ψ	Set of BSs	
i, j, b	BS number (or cell number)	$i \in \Psi$, $j \in \Psi$, $b \in \Psi$
$\mathcal{N}_b$	Set of UEs attached to the b-th BS	
k_b	k-th UE attached to the b-th BS	$k_b \in \mathcal{N}_b$
Ω_b^{DL}	Set of additional DL-UE newly allocated in the n-th subframe (ULSF in HD) by IBFD among the UEs attached to the b-th BS	$\Omega_b^{\mathrm{DL}} \subset \mathcal{N}_b$
Ω_b^{UL}	Set of additional UL-UE newly allocated in the m-th subframe (DLSF in HD) by IBFD among the UEs attached to the b-th BS	$\Omega_b^{\mathrm{UL}} \subset \mathcal{N}_b$
m	Subframe number (DLSF in HD)	
n	Subframe number (ULSF in HD)	
d_b	DL-UE attached to the b-th BS	
u_b	UL-UE attached to the b-th BS	
$P_{y,x}$	Received power at the y-th BS or UE for the signal transmitted by the x-th BS or UE	
P_x	Transmission power of the x-th BS or UE	
$P_{\mathrm{BS}}^{\mathrm{ULSF}}$	BS transmission power in ULSF	
$P_{\mathrm{BS}}^{\mathrm{DLSF}}$	BS transmission power in DLSF	
$P_{\mathrm{UE}}^{\max}$	Maximum UE transmission power	
$P_{\mathrm{UE}}^{\lim}$	UE transmission power limit for UL-UE scheduling in DLSF-DDC	
G_x	Antenna gain of the x-th BS or UE	
$L_{y,x}$	Propagation loss between the x-th BS or UE and the y-th BS or UE	
N_y	Noise power at the y-th BS or UE	
$I_{y,x}$	Interference power at the y-th BS or UE received from the signal transmitted by the x-th BS or UE	
I^{SI}	Residual SI power at the b-th BS	$I^{\mathrm{SI}} = I_{b,b}$
I^{B}	A sum of interferences received by the x-th UE or BS from BSs in neighboring cells	
I^{U}	A sum of interferences received by the x-th UE or BS from all UEs transmitting signals	
$\gamma_{y,x}^{\mathrm{HD}}$	SINR from the x-th BS or UE to the y-th BS or UE when the system is operated by HD	
$\gamma_{y,x}^{\mathrm{FD}}$	SINR from the x-th BS or UE to the y-th BS or UE when IBFD is applied	
$R^{\mathrm{DL}}(k_b, m)$	Instantaneous DL throughput of the k -th UE when the k -th UE is assigned to the m-th subframe	
$\overline{R^{\mathrm{DL}}}(k_b, m)$	Averaged DL throughput of the k -th UE in the m-th subframe, averaged over the number of subframes, M	
$R^{\mathrm{UL}}(k_b, m)$	Instantaneous UL throughput of the k -th UE when the k -th UE is assigned to the m-th subframe	
$\overline{R^{\mathrm{UL}}}(k_b, m)$	Averaged UL throughput of the k -th UE in the m-th subframe, averaged over the number of subframes, M	
$\omega_{y,x}^{\mathrm{MODE}}$	CQI corresponding to the SINR of $\gamma_{y,x}^{\mathrm{MODE}}$, MODE $\in$ {HD, FD}	

II. DUPLEX SCHEMES FOR CELLULAR SYSTEMS

A. HALF-DUPLEX WITH STATIC-TDD

Existing 3GPP-compliant cellular systems employ HD-based DL/UL allocation, in which DL and UL communications are independently allocated to radio resources (e.g., TDD or FDD) to avoid interference. An example of a TDD-based allocation (static-TDD) is shown in Fig. 3(a). To mitigate ICIs, the allocation of either DL or UL communications in each subframe is the same for all cells. Thus, in the downlink subframe (DLSF), UEs receive ICIs from BSs in adjacent cells, but not from UEs in adjacent cells, as shown in Fig. 4(a). Similarly, in the uplink subframe (ULSF), BSs receive ICIs from UEs in adjacent cells, but not from BSs in adjacent cells, as shown in Fig. 5(a). However, in this general TDD-based cellular system, the UL/DL allocation pattern for the subframes cannot be changed for each cell. Therefore, flexibly

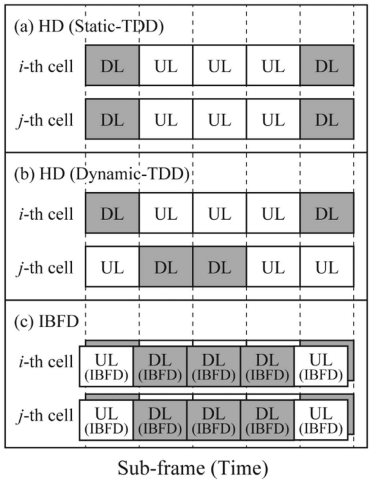

FIGURE 3. Duplex schemes for cellular systems.

responding to the UE communication requests in each cell is impossible.

B. HALF-DUPLEX WITH DYNAMIC-TDD

Dynamic TDDs have been utilized in recent years to respond flexibly to different UE communication requests for each cell [40], [41], [42]. As shown in Fig. 3(b), each cell operates with TDD; however, allows different DLSF/ULSF assignments for each cell. Although flexible subframe allocation is possible, additional ICIs may be observed between BSs and UEs in different cells.

C. IN-BAND FULL-DUPLEX

IBFD has attracted significant attention as a method that can theoretically double the spectral efficiency of conventional HD systems because it simultaneously performs UL and DL communications, as shown in Figs. 2 and 3(c). However, many challenges must be overcome to introduce IBFD into a cellular system, including new interferences, such as SI, IUI, and ICIs.

Many studies on SI cancellation methods have been reported, mainly in the antenna, analog, and digital domains, and the feasibility of achieving an SI cancellation performance of approximately 110 dB is increasing [16], [17], [18], [19], [20], [21], [22], [23], [24], [25], [26], [27], [28], [29], [30], [31], [32], [33], [34]. In addition, the implementation size, computational complexity, and power consumption of such an SI canceller are yet to be addressed. However, because the SI canceller is implemented on the BS side, it is expected to be considerably tolerable. Various methods to realize IUI cancellation have been proposed [35]. However, problems such as the reduction of computational complexity, realization of IUI cancellation with implementation size, and low power consumption that can be implemented in a smartphone remain unresolved.

As explained in Section III, the individual cancellation of ICIs is impractical because they originate from a large number of BSs and UEs in neighboring cells. Therefore, scheduling methods, such as the sum rate-maximizing algorithm have been proposed [36], [37], [38], [39]. However, most of these methods assume that IBFD is implemented only in a single cell [36], [37], [38] or in the central cell of a multi-cell [39]. Practical methods to implement the IBFD in all cells have not been established. A smooth transition to a system that applies IBFD to the current cellular system employing static or dynamic-TDD has not been established, which renders the practical application of FDC problematic.

III. PROPOSED DYNAMIC FULL-DUPLEX CELLULAR SYSTEM

Here, we examine the concept and principle of the proposed DDC system, as well as the scheduling and power control methods to realize the DDC system.

A. CONCEPTS AND PRINCIPLES

The proposed DDC system is based on an existing TDD-based cellular system. First, the DL-UE and UL-UE are determined from the set of candidate UEs attached to the b-th BS by utilizing the scheduling algorithm in the DLSF and ULSF, respectively, as shown in Fig. 6(a). Second, IBFD is applied only to subframes that have a limited impact on the already-allocated TDD communications, and the communications of the new UEs are added, as shown in Fig. 6(b)–(d). We analyze three scenarios: IBFD is dynamically applied only to DLSFs (DLSF-DDC shown in Fig. 6(b)), only to ULSFs (ULSF-DDC shown in Fig. 6(c)), and to all subframes (DDC shown in Fig. 6(d)).

1) DLSF-DDC

In the case of DLSF-DDC, IBFD is dynamically applied only to DLSFs, as shown in Fig. 6(b). IBFD is applied if the new interference generated by the additional UL communications with the IBFD is less than a certain level of impact on the quality of the existing TDD-DL communications. Therefore, we provided the interference models in the DLSF without and with IBFD.

The interference model in the i-th cell for the m-th DLSF without IBFD application is shown in Fig. 4(a). For simplicity, only the j-th cell is shown as an adjacent cell. All cells are assumed to utilize the same frequency. Therefore, the d_i-th DL-UE receives the desired signal transmitted from the i-th BS and the interferences transmitted from the $\{\psi \setminus i\}$-th BSs located in the other cells. Here $\{\psi \setminus i\}$ means the set ψ that does not contain i. Thus, the signal-to-interference plus noise power ratio (SINR) of the DL communication at the d_i-th DL-UE in the m-th DLSF without IBFD application, $\gamma^{\mathsf{HD}}_{d_i,i}$, can be expressed as follows:

$$\gamma^{\mathsf{HD}}_{d_i,i} = \frac{P_{d_i,i}}{N_{d_i} + I^{\mathsf{B}}_{d_i}}, \tag{1}$$

$$I^{\mathsf{B}}_{d_i} = \sum_{b\in\{\psi\setminus i\}} I_{d_i,b}\,, \tag{2}$$

$$P_{d,b} = G_d L_{d,b} G_b P_b. \tag{3}$$

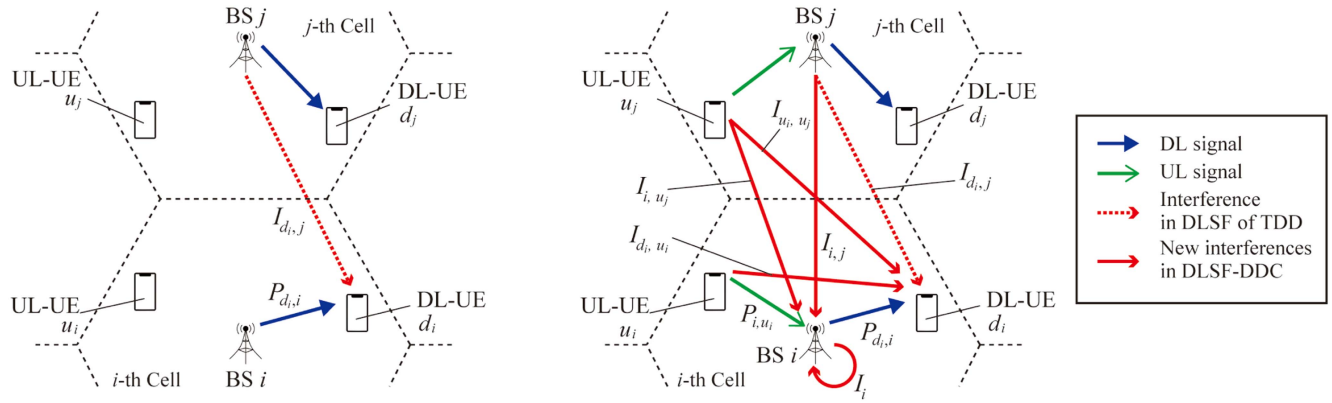

(a) Interference in DLSF without IBFD application. (b) Interference in DLSF with IBFD application.

FIGURE 4. **Interference models in the *i*-th cell for the DLSF (for simplicity, only the *j*-th cell is shown as the adjacent cell).**

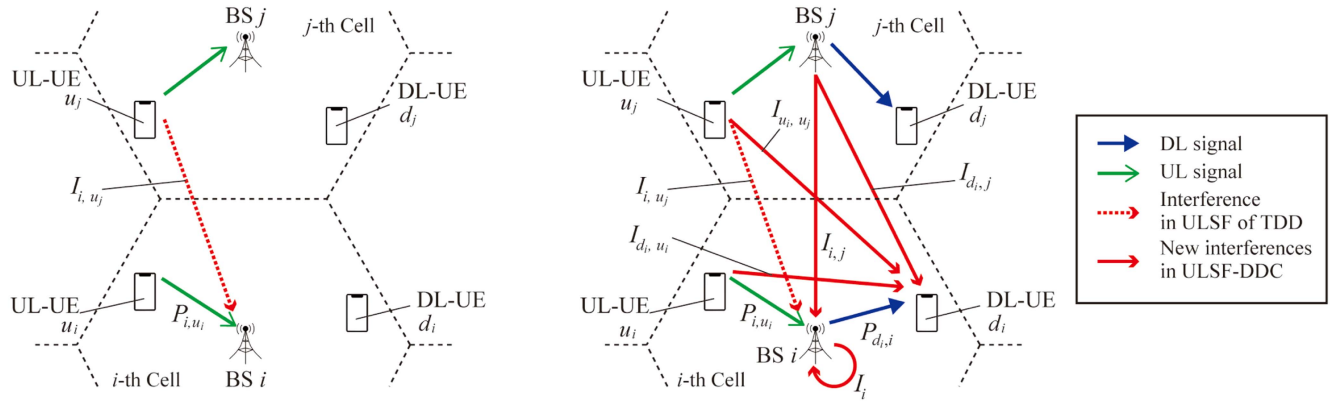

(a) Interference in ULSF without IBFD application. (b) Interference in ULSF with IBFD application.

FIGURE 5. **Interference models in the *i*-th cell for the ULSF (for simplicity, only the *j*-th cell is shown as the adjacent cell).**

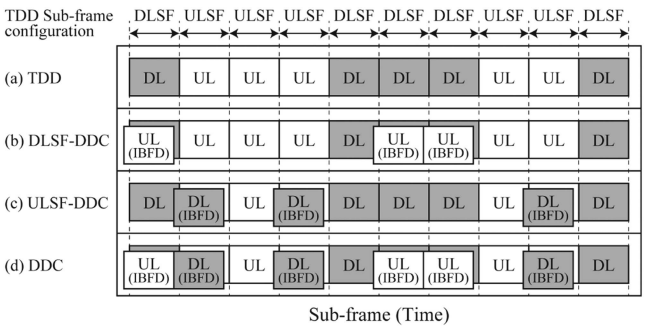

FIGURE 6. **TDD subframe configuration and allocation of DL/UL communication in each scheme.**

The interference model in the i-th cell for the m-th DLSF with the IBFD application is shown in Fig. 4(b). Suppose IBFD can be applied. In that case, the UL communications transmitted by the u_b-th UL-UEs are added to the DLSF. These additional UL signals represent new interferences for the d_i-th DL-UE, as shown in Fig. 4(b). Therefore, the SINR of the DL communication at the d_i-th DL-UE in DLSF with IBFD application, $\gamma^{\mathsf{FD}}_{d_i,i}$, can be expressed as follows:

$$\gamma^{\mathsf{FD}}_{d_i,i} = \frac{P_{d_i,i}}{N_{d_i} + I^{\mathsf{B}}_{d_i} + I^{\mathsf{U}}_{d_i}}, \tag{4}$$

$$I^{\mathsf{U}}_{d_i} = \sum_{b\in\{\psi\}} \sum_{u_b\in\{\Omega^{\mathsf{UL}}_b\}} I_{d_i,u_b}\,. \tag{5}$$

When $\Omega^{\mathsf{UL}}_b = \emptyset$, no UL-UE candidate can be superimposed by IBFD on the already assigned DL communication in the b-th cell. Therefore, the following should be defined:

$$\sum_{x\in\emptyset} I_{y,x} = 0. \tag{6}$$

In contrast, the i-th BS receives interferences from its own transmission signal (i.e., SI), other cell superimposed UL-UEs, and other cell BS. Suppose an IBFD-applicable UL-UE exists in the i-th cell. In that case, the SINR of the UL communication at the i-th BS in the m-th DLSF, $\gamma^{\mathsf{FD}}_{i,u_i}$, can be

expressed as follows:

$$\gamma^{\mathsf{FD}}_{i,\,u_i} = \frac{P_{i,u_i}}{N_i + I^{\mathsf{B}}_i + I^{\mathsf{SI}}_i + \left(I^{\mathsf{U}}_i - P_{i,u_i}\right)}. \tag{7}$$

Algorithms to determine the set of IBFD-applicable UL-UE candidates, Ω^{UL}_b, and appropriate transmission power control are required to improve the system throughput of the conventional TDD-based cellular system by DLSF-DDC.

2) ULSF-DDC

In the case of the ULSF-DDC, IBFD is dynamically applied only to ULSFs, as shown in Fig. 6(c). IBFD is applied if the new interference generated by the additional DL communications with the IBFD is less than a certain level of impact on the quality of the existing TDD-UL communications. Therefore, we provided the interference models in ULSF without and with IBFD.

The interference model in the i-th cell for the n-th ULSF without IBFD application is shown in Fig. 5(a). For simplicity, only the j-th cell is shown as an adjacent cell. The i-th BS receives the desired signal transmitted from the u_i-th UL-UE and the interferences transmitted from the u_b-th UL-UEs ($b \in \psi \setminus i$) located in other cells. Thus, the SINR of the UL communication at the i-th BS in ULSF without IBFD application, $\gamma^{\mathsf{HD}}_{i,u_i}$, can be expressed as follows:

$$\gamma^{\mathsf{HD}}_{i,u_i} = \frac{P_{i,u_i}}{N_i + \left(I^{\mathsf{U}}_i - P_{i,u_i}\right)}. \tag{8}$$

The interference model in the i-th cell for the n-th ULSF with the IBFD application is shown in Fig. 5(b). Suppose the IBFD can be applied. In that case, DL communications from the b-th BS to the d_b-th DL-UE are added to the ULSF. When $\Omega^{\mathsf{DL}}_b = \emptyset$, no DL-UE candidate can be superimposed by IBFD on the already assigned UL communication in the b-th cell. When $\Omega^{\mathsf{DL}}_b \neq \emptyset$, the additional DL signals cause new interferences, as shown in Fig. 5(b). The i-th BS additionally receives interferences from the other cell's b-th BSs ($b \in \psi \setminus i$). Therefore, the SINR of the UL communication at the i-th BS in ULSF with IBFD application, $\gamma^{\mathsf{FD}}_{i,u_i}$, can be expressed as (7).

In contrast, the d_i-th DL-UE receives interferences from its own and u_b-th UL-UEs of other cells ($b \in \psi$) as well as interferences from the b-th BS of other cells ($b \in \psi \setminus i$). Therefore, the SINR of the DL communication at the i-th BS in ULSF, $\gamma^{\mathsf{FD}}_{d_i,i}$, can be expressed as (4) provided an IBFD-applicable DL-UE exists in the i-th cell.

To improve the system throughput of the conventional TDD-based cellular system by ULSF-DDC, algorithms to determine the set of IBFD-applicable DL-UE candidates, Ω^{DL}_b, and appropriate transmission power control are required.

3) DDC

In the case of the DDC, all subframes are candidates for the application of IBFD. As shown in Fig. 6(d), the IBFD is applied provided the impact of the new interference generated by additional DL/UL communications with the IBFD on the quality of the existing TDD-UL/-DL communication is less than a certain level. That is, the DLSF-DDC and ULSF-DDC system models are applied to the DLSF and ULSF, respectively.

Algorithm 1: UE Scheduling in the m-th Subframe (DLSF).

1: Calculate SINR information $\gamma^{\mathsf{HD}}_{d_i,i}$ for all attached UEs $\mathcal{N}_b$;
2: Map all calculated SINR information $\gamma^{\mathsf{HD}}_{d_i,i}$ to CQI $\omega^{\mathsf{HD}}_{d_i,i}$;
3: **for** $k_i = 1$ to $|\mathcal{N}_i|$ **do**
4: Calculate $\overline{R^{\mathsf{DL}}}(k_i, m-1)$ according to (10);
5: Calculate $R^{\mathsf{DL}}(k_i, m)$ using $\omega^{\mathsf{HD}}_{d_i,i}$;
6: **end for**
7: Obtain DL-UE d_i according to (9);
8: Calculate SINR information $\gamma^{\mathsf{FD}'}_{d_i,i}$ and $\gamma^{\mathsf{FD}'}_{i,\,u_i}$ for all attached UEs $\mathcal{N}_i$;
9: Map all calculated SINR information $\widehat{\gamma^{\mathsf{FD}}_{d_i,i}}$ and $\widehat{\gamma^{\mathsf{FD}}_{i,\,u_i}}$ to CQI $\widehat{\omega^{\mathsf{FD}}_{d_i,i}}$ and $\widehat{\omega^{\mathsf{FD}}_{i,\,u_i}}$, respectively;
10: Initialize Ω^{UL}_i as $\emptyset$;
11: **for** $k_i = 1$ to $|\mathcal{N}_i| - 1$ **do**
12: **if** $\omega^{\mathsf{HD}}_{d_i,i} - \widehat{\omega^{\mathsf{FD}}_{d_i,i}}(k_i) > 0$ **then**
13: **if** $P_{k_i} \leq P^{\mathsf{lim}}_{\mathsf{UE}}$ **then**
14: $\Omega^{\mathsf{UL}}_i = \Omega^{\mathsf{UL}}_i \cup \{k_i\}$;
15: **end if**
16: **end if**
17: **end for**
18: **if** $\Omega^{\mathsf{UL}}_i \neq \emptyset$ **then**
19: **for** $k_i = 1$ to $|\Omega^{\mathsf{UL}}_i|$ **do**
20: Calculate $\overline{R^{\mathsf{UL}}}(\Omega^{\mathsf{UL}}_i(k_i), m-1)$ according to (14);
21: Calculate $R^{\mathsf{UL}}(\Omega^{\mathsf{UL}}_i(k_i), m)$ using $\widehat{\omega^{\mathsf{FD}}_{i,\,u_i}}$;
22: **end for**
23: Obtain UL-UE u_i according to (13);

B. SCHEDULING

The proposed DDC system apply an extended UE scheduling algorithm based on proportional fairness scheduling (PFS) to apply the IBFD while maintaining compatibility with conventional HD cellular systems. The SINR information that can be collected by the b-th BS is limited to that related to UEs in its own cell, and the information from other cells cannot be utilized for scheduling.

1) SCHEDULING FOR DLSF-DDC

The scheduling flow of the proposed DDC system when the m-th subframe is a DLSF is shown in Algorithm 1. First, as in conventional TDD-based cells, the DL-UEs are selected by utilizing the PFS in each cell, and communication resources

are allocated. The channel quality indicator (CQI), $\omega^{\mathsf{HD}}_{d_i,i}$, corresponding to the SINR, $\gamma^{\mathsf{HD}}_{d_i,i}$, measured at the d_i-th DL-UE ($d_i \in \Omega_i$) is fed back to the i-th BS, which utilizes this CQI to operate the PFS. In the i-th cell, the DL-UE, d_i, to which communication is assigned in the m-th DLSF, is determined by utilizing the PFS as follows:

$$d_i = \arg\max_{k_i \in \mathcal{N}_i} \frac{R^{\mathsf{DL}}(k_i, m)}{\overline{R^{\mathsf{DL}}}(k_i, m-1)}, \tag{9}$$

$$\overline{R^{\mathsf{DL}}}(k_i, m) = \left(1 - \frac{1}{M}\right)\overline{R^{\mathsf{DL}}}(k_i, m-1) + \frac{p(k_i, m)}{M} R^{\mathsf{DL}}(k_i, m), \tag{10}$$

where $R^{\mathsf{DL}}(k_i, m)$ is the instantaneous DL throughput of the k_i-th UE when the k_i-th UE is assigned to the m-th subframe, calculated by utilizing the modulation and coding scheme (MCS) index corresponding to the measured CQI, $\omega^{\mathsf{HD}}_{k_i,i}$. $\overline{R^{\mathsf{DL}}}(k_i, m)$ is the DL throughput of the k_i-th UE in the m-th subframe, averaged over the number of subframes M. Here, $p(k_i, m) = 1$ indicates that the k_i-th UE is assigned to the m-th subframe and communication was successful; otherwise, $p(k_i, m) = 0$.

Next, the UL-UE to be added by IBFD is determined. The proposed DDC system does not utilize the UE allocation information of other cells; therefore, scheduling can be performed by utilizing only the information that can be collected to a practical extent. That is, $I^{\mathsf{U}}_{d_i}$ and $(I^{\mathsf{U}}_i - P_{i,u_i})$ cannot be utilized in the calculation. Therefore, the SINR information utilized for scheduling $\gamma^{\mathsf{FD}}_{d_i,i}$ and $\gamma^{\mathsf{FD}}_{i,\,u_i}$ in (4) and (7) are modified as follows, omitting interference related to UEs allocated in other cells:

$$\widehat{\gamma^{\mathsf{FD}}_{d_i,i}}(u_i) = \frac{P_{d_i,i}}{N_{d_i} + I^{\mathsf{B}}_{d_i} + I_{d_i,u_i}}, \tag{11}$$

$$\widehat{\gamma^{\mathsf{FD}}_{i,\,u_i}} = \frac{P_{i,u_i}}{N_i + I^{\mathsf{B}}_i + I^{\mathsf{SI}}_i}. \tag{12}$$

Here are examples of how $I^{\mathsf{B}}_{d_i}$, I^{B}_i, and I_{d_i,u_i} are measured. Generally, UEs constantly monitor the signal quality from neighboring BSs in preparation for handover. Therefore, the signal power received from neighboring BSs ($I^{\mathsf{B}}_{d_i}$) can be easily monitored by UEs. Next, as BSs are fixedly installed and have fixed transmission power, the i-th BS can easily monitor the interference power between BSs (I^{B}_i) by pre-measurement or by periodic measurement of synchronization signals and physical broadcast channel (SS/PBCH) blocks transmitted by neighboring BSs. Finally, when a UE is not transmitting its own UL signal in the ULSF, the UE receives demodulation reference signals (DM-RSs) from another UE, measures its power (I_{d_i,u_i}), and reports the measurement power information to the BS. Upon receiving the report, the BS can determine the interference power between each UE by referring to the reported information and the UE resource allocation map.

Thus, the CQIs, $\widehat{\omega^{\mathsf{FD}}_{d_i,i}}(u_i)$, and $\widehat{\omega^{\mathsf{FD}}_{i,\,u_i}}$, corresponding to the SINRs, $\widehat{\gamma^{\mathsf{FD}}_{d_i,i}}(u_i)$, and $\widehat{\gamma^{\mathsf{FD}}_{i,\,u_i}}$, are calculated, respectively. In the proposed system, new communications are superimposed on the IBFD only when the communications allocated to the HD are slightly or not affected. Therefore, u_i-th UEs that satisfied the conditions $\omega^{\mathsf{HD}}_{d_i,i} - \widehat{\omega^{\mathsf{FD}}_{d_i,i}}(u_i) > 0$ are candidates for additional allocation by IBFD. Furthermore, interference from other cell UEs cannot be utilized in the calculation of $\widehat{\omega^{\mathsf{FD}}_{d_i,i}}(u_i)$; thus, an appropriate upper limit on UE transmission power, $P^{\mathsf{lim}}_{\mathsf{UE}}$, should be set to minimize the impact of this interference. Therefore, among the candidate terminals earlier mentioned, u_i-th UEs whose transmission power are below the power limit, $P^{\mathsf{lim}}_{\mathsf{UE}}$, are the final candidates, Ω^{UL}_i, for additional allocation by the IBFD. The upper limit of the UE transmission power, $P^{\mathsf{lim}}_{\mathsf{UE}}$, is determined in advance through computer simulations.

Therefore, the additional UL-UE u_i, to which communication is assigned in the m-th DLSF, is determined by utilizing the PFS as follows:

$$u_i = \arg\max_{k_i \in \Omega^{\mathsf{UL}}_i} \frac{R^{\mathsf{UL}}\left(\Omega^{\mathsf{UL}}_i(k_i), m\right)}{\overline{R^{\mathsf{UL}}}\left(\Omega^{\mathsf{UL}}_i(k_i), m-1\right)}, \tag{13}$$

$$\overline{R^{\mathsf{UL}}}\left(\Omega^{\mathsf{UL}}_i(k_i), m\right) = \left(1 - \frac{1}{M}\right)\overline{R^{\mathsf{UL}}}\left(\Omega^{\mathsf{UL}}_i(k_i), m-1\right) + \frac{p\left(\Omega^{\mathsf{UL}}_i(k_i), m\right)}{M} R^{\mathsf{UL}}\left(\Omega^{\mathsf{UL}}_i(k_i), m\right), \tag{14}$$

where $R^{\mathsf{UL}}(k_i, m)$ is the instantaneous UL throughput of the k_i-th UE when the k_i-th UE is assigned to the m-th subframe, calculated by utilizing the CQI, $\widehat{\omega^{\mathsf{FD}}_{d_i,i}}$. $\overline{R^{\mathsf{UL}}}(k_i, m)$ is the UL throughput of the k_i-th UE in the m-th subframe, averaged over the number of subframes, M.

2) SCHEDULING FOR ULSF-DDC

The scheduling flow of the proposed DDC system when the n-th subframe is a ULSF is shown in Algorithm 2. First, as in conventional TDD-based cells, UL-UEs are selected by utilizing the PFS in each cell, and communication resources are allocated. Because the UE allocation information for other cells cannot be utilized, scheduling is performed by utilizing only information that can be collected to an extent that is practical. That is, $(I^{\mathsf{U}}_i - P_{i,u_i})$ cannot be utilized in the calculations. Therefore, the SINR information utilized for scheduling $\gamma^{\mathsf{HD}}_{i,u_i}$ in (8) is modified as follows:

$$\widehat{\gamma^{\mathsf{HD}}_{i,u_i}} = \frac{P_{i,u_i}}{N_i + \left(\widehat{I^{\mathsf{U}}_i} - P_{i,u_i}\right)}, \tag{15}$$

where $\widehat{I^{\mathsf{U}}_i}$ is the assumed interference power. The average value of the total interference power calculated multiple times through computer simulation for the case in which UL-UEs are randomly placed in other cells is utilized as $\widehat{I^{\mathsf{U}}_i}$. The CQI, $\widehat{\omega^{\mathsf{HD}}_{i,u_i}}$, corresponding to the SINR, $\widehat{\gamma^{\mathsf{HD}}_{i,u_i}}$, is assumed at the i-th

BS to operate the PFS. In the i-th cell, the UL-UE u_i, to which communication is assigned in the n-th ULSF, is determined by utilizing the PFS as follows:

$$u_i = \arg\max_{k_i \in \mathcal{N}_i} \frac{R^{\mathsf{UL}}(k_i, n)}{\overline{R^{\mathsf{UL}}}(k_i, n-1)}, \tag{16}$$

$$\overline{R^{\mathsf{UL}}}(k_i, n) = \left(1 - \frac{1}{M}\right)\overline{R^{\mathsf{UL}}}(k_i, n-1) + \frac{p(k_i, n)}{M} R^{\mathsf{UL}}(k_i, n). \tag{17}$$

Subsequently, the DL-UE to be added by the IBFD is determined. The proposed DDC system does not utilize the UE allocation information of other cells; therefore, scheduling can be performed by utilizing only the information that can be collected to a practical extent. Therefore, the SINR information utilized for scheduling $\gamma^{\mathsf{FD}}_{i,\,u_i}$ and $\gamma^{\mathsf{FD}}_{d_i,i}$ in (7) and (4) are modified as follows, omitting the interference related to UEs allocated in other cells:

$$\widehat{\gamma^{\mathsf{FD}}_{i,\,u_i}} = \frac{P_{i,u_i}}{N_i + \beta I^{\mathsf{B}}_i + I^{\mathsf{SI}}_i + \left(\widehat{I^{\mathsf{U}}_i} - P_{i,u_i}\right)}, \tag{18}$$

$$\widehat{\gamma^{\mathsf{FD}}_{d_i,i}} = \frac{P_{d_i,i}}{N_{d_i} + I^{\mathsf{B}}_{d_i} + \widehat{I^{\mathsf{U}}_{d_i}}}. \tag{19}$$

where β is an adjustment factor for the total interference power from BSs in other cells to be considered in scheduling. $\widehat{I^{\mathsf{U}}_{d_i}}$ is the assumed interference power obtained through computer simulations when obtaining $\widehat{I^{\mathsf{U}}_i}$. Thus, the CQIs, $\widehat{\omega^{\mathsf{FD}}_{i,\,u_i}}$, and $\widehat{\omega^{\mathsf{FD}}_{d_i,i}}$, corresponding to the SINRs, $\widehat{\gamma^{\mathsf{FD}}_{i,\,u_i}}$, and $\widehat{\gamma^{\mathsf{FD}}_{d_i,i}}$, are calculated, respectively. In the proposed system, new communications are superimposed on the IBFD only when communications allocated to the HD are slightly or not affected. Therefore, d_i-th UEs that satisfy the conditions $\widehat{\omega^{\mathsf{HD}}_{i,u_i}} - \widehat{\omega^{\mathsf{FD}}_{i,\,u_i}} > 0$ are candidates for additional allocation by utilizing the IBFD.

Thus, the additional DL-UE, d_i, to which communication is assigned in the n-th ULSF, is determined by utilizing the PFS, as follows:

$$d_i = \arg\max_{k_i \in \Omega^{\mathsf{DL}}_i} \frac{R^{\mathsf{DL}}\left(\Omega^{\mathsf{DL}}_i(k_i), n\right)}{\overline{R^{\mathsf{DL}}}\left(\Omega^{\mathsf{DL}}_i(k_i), n-1\right)}, \tag{20}$$

$$\overline{R^{\mathsf{DL}}}\left(\Omega^{\mathsf{DL}}_i(k_i), n\right) = \left(1 - \frac{1}{M}\right)\overline{R^{\mathsf{DL}}}\left(\Omega^{\mathsf{DL}}_i(k_i), n-1\right) + \frac{p\left(\Omega^{\mathsf{DL}}_i(k_i), n\right)}{M} R^{\mathsf{DL}}\left(\Omega^{\mathsf{DL}}_i(k_i), n\right). \tag{21}$$

C. TRANSMISSION POWER CONTROL FOR UES

In 3GPP-compliant cellular systems, UE transmission power control is specified according to the estimated propagation loss between the BS and UE to efficiently suppress UE power consumption and ICI [43]. In this study, open-loop control is applied to UE transmission power control, assuming no time variability of the communication traffic and received power. The transmission power of the u_i-th UE is expressed as follows:

$$P_{u_i} = \min\left\{P_0 + 10\log_{10}L + \alpha\Gamma_{i,u_i}, P^{\mathsf{max}}_{\mathsf{UE}}\right\}, \tag{22}$$

where P_0, L, Γ_{i,u_i}, α, and $P^{\mathsf{max}}_{\mathsf{UE}}$ represent the target received signal power per resource block (RB), number of allocated RBs, estimated propagation loss between the i-th BS and u_i-th UE, compensation factor for the propagation loss, and maximum transmission power of the UE, respectively.

Algorithm 2: UE Scheduling in the n-th Subframe (ULSF).

1: Calculate the SINR information $\widehat{\gamma^{\mathsf{HD}}_{i,u_i}}$ for all attached UEs $\mathcal{N}_b$;
2: Map all calculated SINR information $\widehat{\gamma^{\mathsf{HD}}_{i,u_i}}$ to CQI $\widehat{\omega^{\mathsf{HD}}_{i,u_i}}$;
3: **for** $k_i = 1$ to $|\mathcal{N}_i|$ **do**
4: Calculate $\overline{R^{\mathsf{UL}}}(k_i, n-1)$ according to (17);
5: Calculate $R^{\mathsf{UL}}(k_i, n)$ by utilizing $\widehat{\omega^{\mathsf{HD}}_{i,u_i}}$;
6: **end for**
7: Obtain UL-UE u_i according to (16);
8: Calculate the SINR information $\widehat{\gamma^{\mathsf{FD}}_{i,\,u_i}}$ and $\widehat{\gamma^{\mathsf{FD}}_{d_i,i}}$ for all attached UEs $\mathcal{N}_i$;
9: Map all calculated SINR information $\widehat{\gamma^{\mathsf{FD}}_{i,\,u_i}}$ and $\widehat{\gamma^{\mathsf{FD}}_{d_i,i}}$ to CQI $\widehat{\omega^{\mathsf{FD}}_{i,\,u_i}}$ and $\widehat{\omega^{\mathsf{FD}}_{d_i,i}}$, respectively;
10: Initialize Ω^{DL}_i as $\emptyset$;
11: **for** $k_i = 1$ to $|\mathcal{N}_i| - 1$ **do**
12: **if** $\widehat{\omega^{\mathsf{HD}}_{i,u_i}} - \widehat{\omega^{\mathsf{FD}}_{i,\,u_i}} > 0$ **then**
13: $\Omega^{\mathsf{UL}}_i = \Omega^{\mathsf{UL}}_i \cup \{k_i\}$;
14: **end if**
15: **end for**
16: **if** $\Omega^{\mathsf{DL}}_i \neq \emptyset$ **then**
17: **for** $k_i = 1$ to $|\Omega^{\mathsf{DL}}_i|$ **do**
18: Calculate $\overline{R^{\mathsf{DL}}}(\Omega^{\mathsf{DL}}_i(k_i), n-1)$ according to (21);
19: Calculate $R^{\mathsf{DL}}(\Omega^{\mathsf{DL}}_i(k_i), n)$ using $\widehat{\gamma^{\mathsf{FD}}_{d_i,i}}$;
20: **end for**
21: Obtain DL-UE d_i according to (20);

IV. PERFORMANCE EVALUATION

Here, we evaluate the proposed DDC system through computer simulations.

A. SIMULATION CONFIGURATIONS

1) SYSTEM PARAMETERS

During the simulation, the parameters are compliant with those in Table 2. These parameters are based on the dense urban multicell environment specified by 3GPP [44]. The cell configuration utilized for the computer simulation, with 19

TABLE 2. Simulation Parameters

Parameter	Value
Repetition cell layout	19 circle cells
Inter-BS distance	200 m
Carrier frequency	4.0 GHz
Based system	20 MHz-bandwidth TD-LTE [45]
Base duplex scheme	TDD (DL and UL ratio 5:5)
Multiplexing scheme	OFDM (DL and UL)
Channel model	
BS-to-UE, BS-to-BS	3D UMi (Table 7.2-1 in [44])
UE-to-UE	A2.1.2 in TR36.843 [46]
Penetration loss	0 dB
UE moving speed	0 km/h
Fading channel	AWGN
Scheduling scheme	Proportional Fairness Scheduling
Traffic model	Full buffer model
UE distribution	Uniform (20 UEs per cell)
BS maximum transmission power	44 dBm
BS antenna height	10 m
BS antenna pattern	Omnidirectional (5 dBi)
Self-interference cancellation	110 dB
UE maximum transmission power	23 dBm
UE antenna height	1.5 m
UE antenna pattern	Isotropic (0 dBi)

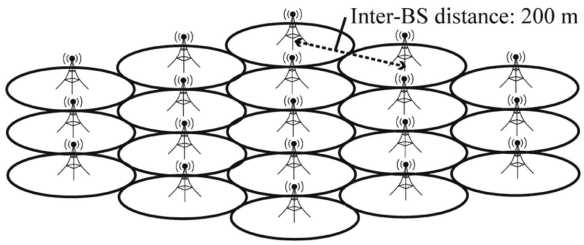

FIGURE 7. Cell configuration for the computer simulation.

cells arranged at an inter-BS distance of 200 m is shown in Fig. 7. Subsequently, cell rapping is performed. In each cell, 20 UEs are uniformly and randomly distributed. Based on assumptions, the channel state information (CSI) can be estimated and its feedback is not delayed. Moreover, all UEs assume a fixed outdoor installation connected to a Wi-SUN FAN border router, and path loss and shadowing are the only channel fluctuations. In addition, the traffic model of the DDC system is assumed to be a full buffer model, assuming that the IoT data aggregated by the Wi-SUN FAN border rooter is very large. In this system-level simulation, the link-level simulator, which is the reference for the SNR-to-block error rate (BLER) curves, is run using TD-LTE with a 20 MHz bandwidth [45]. For all the simulations, the SI is assumed to be ideally reduced by 110 dB at the BS [24].

2) FRAME STRUCTURE

The TDD frame structure based on Configuration #1 defined in the LTE (the basic frame structure of the proposed DDC system) is configured to have the same DLSF and ULSF time ratios, as shown in Fig. 6 [45]. One DLSF or ULSF is assigned to one DL-UE or UL-UE, and the system bandwidth is instantaneously occupied by one UE.

3) EVALUATION METRICS

We utilize four evaluation metrics: the average user throughput, 5% user throughput, IBFD application ratio, and average UL energy of UE per bit (average UL-EPB). The average user throughput is calculated by averaging $\overline{R^{\mathsf{DL}}}$ and $\overline{R^{\mathsf{UL}}}$ shown in (10), (14), (17), and (21) for the overall UEs and all subframes. The 5% user throughput is calculated by sorting the user throughput of all UEs and then obtaining the user throughput of the UE that corresponds to the bottom 5%. The IBFD application ratio is defined as the ratio of subframes to which IBFD has been applied to candidate subframes for the IBFD application. The average UL-EPB, $\bar{\eta}$, is calculated as follows:

$$\bar{\eta} = \frac{\sum_{q=1}^{Q} P_q \times 10^{-3} \cdot T_q \times 10^{-3}}{\sum_{q=1}^{Q} B_q}, \tag{23}$$

where Q is the number of packets, and P_q, T_q, and B_q represent the transmission power (W), time of the q-th packet (s), and size of the q-th packet (bits), respectively [47]. A smaller UL-EPB indicates that the UE is more power efficient in the UL.

B. DLSF-DDC

The performance of the proposed DDC system is evaluated by utilizing a system-level simulation. Here, the DLSF-DDC is evaluated. In the ULSF, P_0 in (22) is set to –90 dBm, which is sufficiently large relative to the thermal noise power, and α is set to 0.8 to balance the average and cell edge user throughputs.

1) EFFECT OF UE TRANSMISSION POWER CONTROL

In the DLSF, throughput and power efficiency are evaluated under different conditions of P_0 and α in the UE transmission power control shown in (22) for UL communications superimposed by IBFD to search for appropriate parameters.

The average user throughput and average UL-EPB as a function of the BS transmission power in the DLSF, $P_{\mathsf{BS}}^{\mathsf{DLSF}}$, are shown in Figs. 8 and 9, respectively, when the UE transmission power limit $P_{\mathsf{UE}}^{\mathsf{lim}}$ is set to 23 dBm (the maximum UE transmission power). As shown in Fig. 8, the average throughput for DL users is superior at $P_0 = -40$ dBm and $\alpha = 0.4$, whereas the average throughput for UL users is approximately the same for all combinations of P_0 and α. In Fig. 9, the average UL-EPB is also the smallest at $\alpha = 0.4$. The assumption of propagation loss between BS and UE increases by decreasing α, thus reducing the transmission power of the UE and suppressing interference from UEs in other cells. Therefore, in terms of efficiency of both throughput and terminal energy consumption, the DLSF-DDC requires P_0 to be set to –40 dBm to obtain a received power sufficiently higher than the interference, and α to be set to 0.4 to suppress interference from UEs in adjacent cells.

2) EFFECT OF UE TRANSMISSION POWER LIMIT

Next, we evaluate the UE transmission power limit, $P_{\mathsf{UE}}^{\mathsf{lim}}$, used for UL-UE scheduling. The average throughput of DL and UL

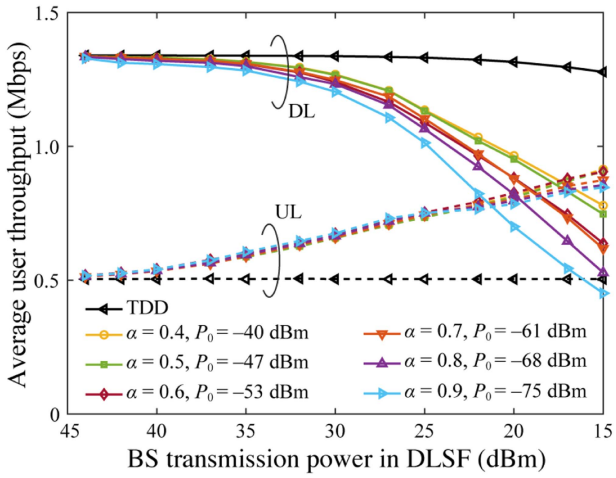

FIGURE 8. Average user throughput as a function of BS transmission power in DLSF for various target received signal powers P_0 and compensation factors for the propagation loss α in DLSF-DDC.

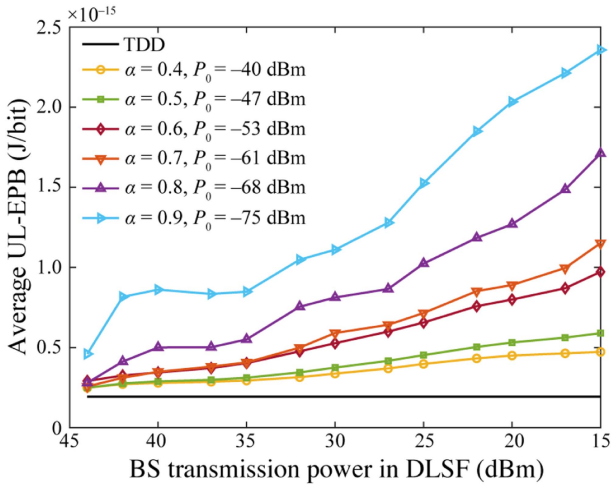

FIGURE 9. Average UL-EPB as a function of BS transmission power in DLSF for various target received signal powers P_0 and compensation factors for the propagation loss α in DLSF-DDC.

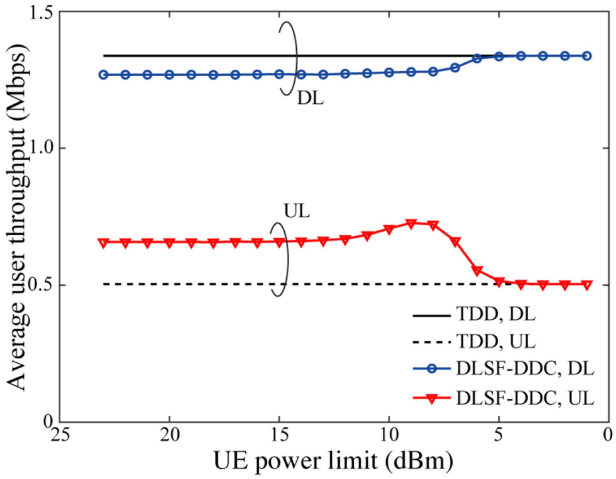

FIGURE 10. Average user throughput as a function of UE transmission power limit $P_{\mathrm{UE}}^{\mathrm{lim}}$ in DLSF-DDC.

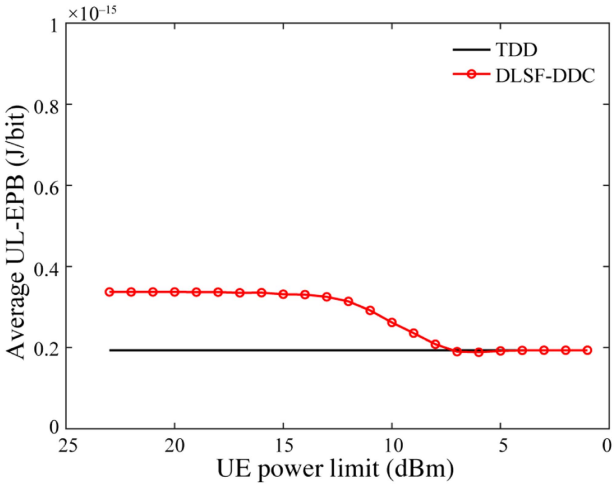

FIGURE 11. Average UL-EPB as a function of the UE transmission power limit $P_{\mathrm{UE}}^{\mathrm{lim}}$ in DLSF-DDC.

communications and average UL-EPB are shown in Figs. 10 and 11, respectively, as a function of $P_{\mathrm{UE}}^{\mathrm{lim}}$ for $P_0 = -40$ dBm, $\alpha = 0.4$, and $P_{\mathrm{BS}}^{\mathrm{DLSF}} = 30$ dBm. When $P_{\mathrm{UE}}^{\mathrm{lim}}$ is 9 dBm, the average UL throughput reaches a maximum, whereas the average DL throughput increases by decreasing $P_{\mathrm{UE}}^{\mathrm{lim}}$. Furthermore, the average UL-EPB is significantly improved by lowering $P_{\mathrm{UE}}^{\mathrm{lim}}$ to less than approximately 13 dBm. This is because UEs with large propagation losses between the BS and UE and transmission power above $P_{\mathrm{UE}}^{\mathrm{lim}}$ are excluded from the UL-UE candidates in the DLSF. Consequently, in addition to the improvement in the UL communication success rate in the DLSF, the average UL-EPB is improved owing to the reduced transmission power of the UL-UE. Based on these results, we set the upper limit of the UE transmission power to $P_{\mathrm{UE}}^{\mathrm{lim}} = 9$ dBm for UL-UE scheduling in the DLSF.

3) EFFECT OF BS TRANSMISSION POWER

The IBFD application ratio as a function of the BS transmission power in the DLSF, $P_{\mathrm{BS}}^{\mathrm{DLSF}}$, when the selected parameters are utilized is shown in Fig. 12. By decreasing $P_{\mathrm{BS}}^{\mathrm{DLSF}}$, the IBFD application ratio increases because interferences from other BSs are suppressed. In addition, the assumed SINR of UL, $\widehat{\gamma_{i,\,u_i}^{\mathrm{FD}}}$, shown in (12) is improved, increasing the number of UEs allocated for UL communication by IBFD in the DLSF.

The average user throughput as a function of $P_{\mathrm{BS}}^{\mathrm{DLSF}}$ is shown in Fig. 13. The UL average user throughput increased by decreasing $P_{\mathrm{BS}}^{\mathrm{DLSF}}$ because the interference from BSs in other cells and the SI are suppressed. Therefore, the assumed UL-SINR, $\widehat{\gamma_{i,\,u_i}^{\mathrm{FD}}}$, shown in (12) is improved, and the CQI, $\widehat{\omega_{i,\,u_i}^{\mathrm{FD}}}$, and IBFD application ratio increases. However, the average DL throughput decreases because the received power of the DL signals decreases. In addition, the interference from the UL-UEs in other cells increases as the IBFD application

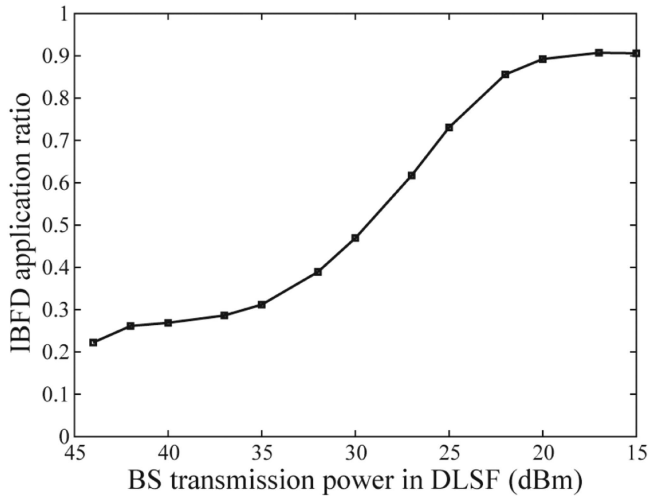

FIGURE 12. IBFD application ratio in DLSF-DDC as a function of BS transmission power.

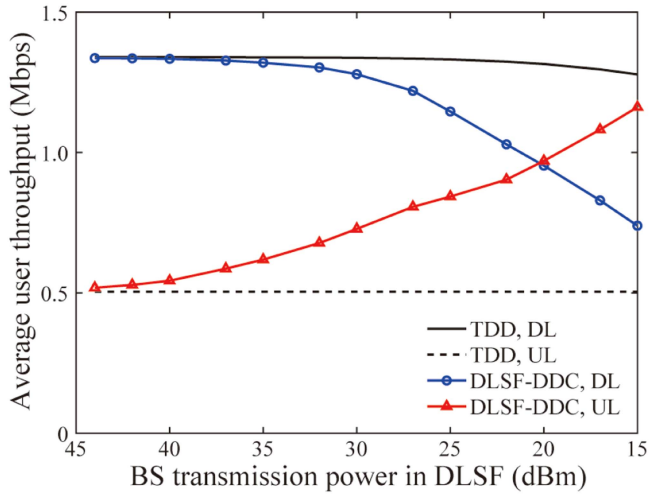

FIGURE 13. Average user throughput as a function of BS transmission power in DLSF-DDC.

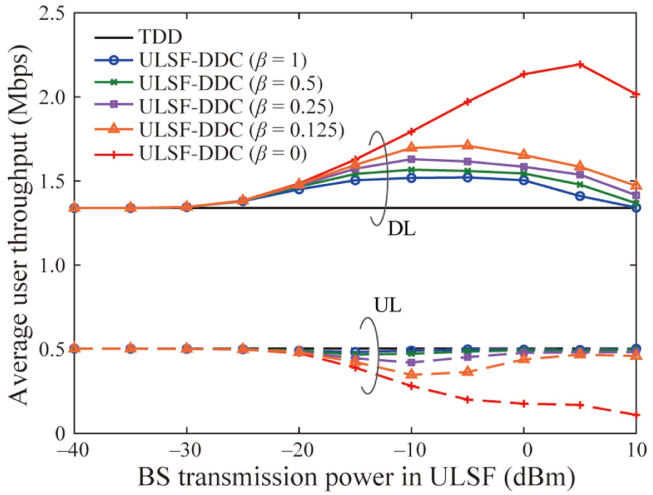

FIGURE 14. Average user throughput as a function of BS transmission power in ULSF for various values of β in ULSF-DDC.

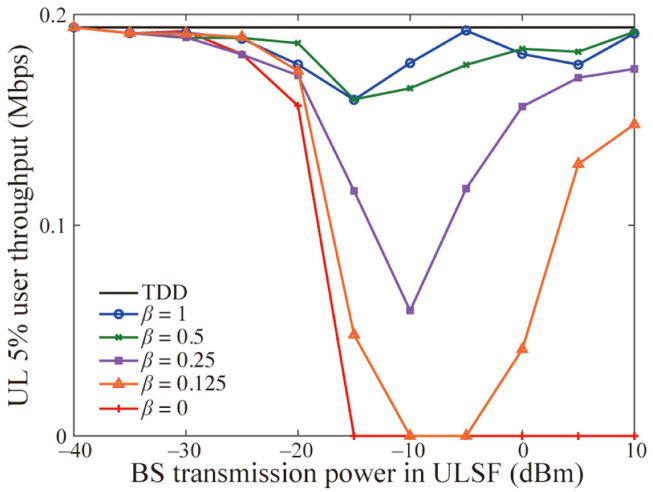

FIGURE 15. UL 5% user throughput as a function of BS transmission power in ULSF for various values of β in ULSF-DDC.

ratio increases, which is unpredictable in the DDC system. In particular, when $P_{\mathrm{BS}}^{\mathrm{DLSF}} = 27$ dBm in the DLSF-DDC, the average UL user throughput can be successfully increased by 60.0% compared with that of the conventional TDD system, whereas the average DL user throughput decreased by only 8.9%.

C. ULSF-DDC

Here, the ULSF-DDC is evaluated. P_0 in (22) is set to –90 dBm, which is sufficiently large relative to the thermal noise power, and α is set to 0.8 to balance the average and cell edge user throughputs. In addition, $P_{\mathrm{BS}}^{\mathrm{DLSF}}$ is set to 44 dBm (maximum BS transmission power).

1) EFFECT OF β ADJUSTMENT

First, the values of β related to the calculation of the assumed UL-SINR, $\widehat{\gamma_{i,u_i}^{\mathrm{FD}}}$, shown in (18) are evaluated. The average user throughput and UL 5% user throughput as a function of the BS transmission power of ULSF, $P_{\mathrm{BS}}^{\mathrm{ULSF}}$, for various β are shown in Figs. 14 and 15, respectively. As β decreases, the average DL user throughput increases and the average UL user throughput decreases. This is because, the conditions for the application of IBFD are relaxed and more DL communications are additionally allocated to the ULSF by decreasing β. Thus, by adjusting β, the system capacity can be expanded in response to traffic. The IBFD application ratio increases when β is less than 0.5. Consequently, the interference from the BSs in other cells increases and the UL 5% user throughput significantly decreases. Therefore, β is set to 0.5 in this study, which improves the average DL user throughput without significantly decreasing the UL 5% user throughput compared with the case where $\beta = 1$.

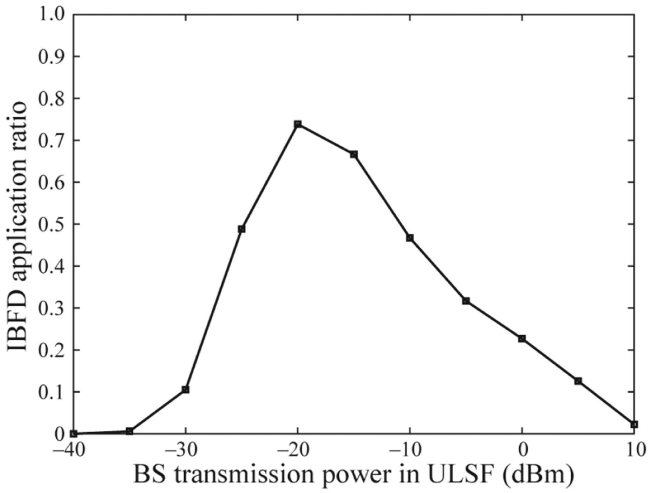

FIGURE 16. IBFD application ratio in the ULSF-DDC as a function of the BS transmission power in the ULSF.

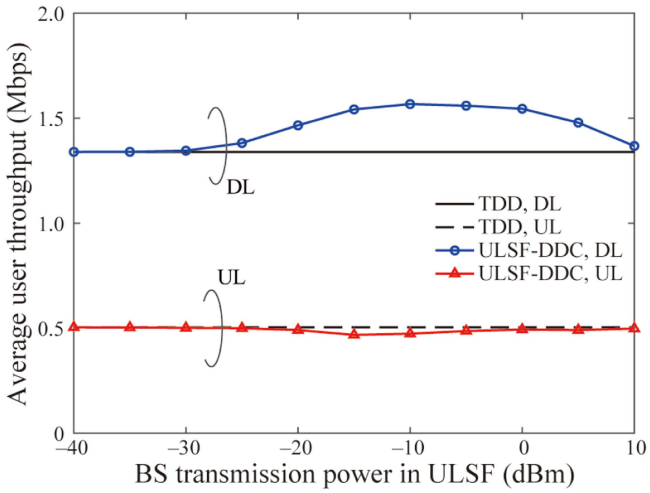

FIGURE 17. Average user throughput as a function of BS transmission power in the ULSF in ULSF-DDC.

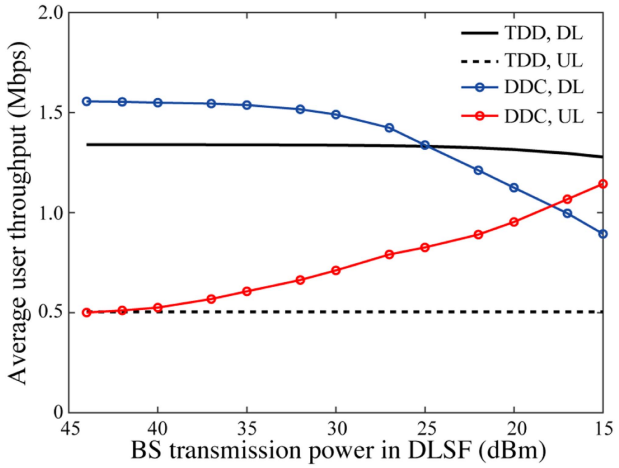

FIGURE 18. Average user throughput as a function of BS transmission power in the DLSF when DDC is applied to both DLSF and ULSF.

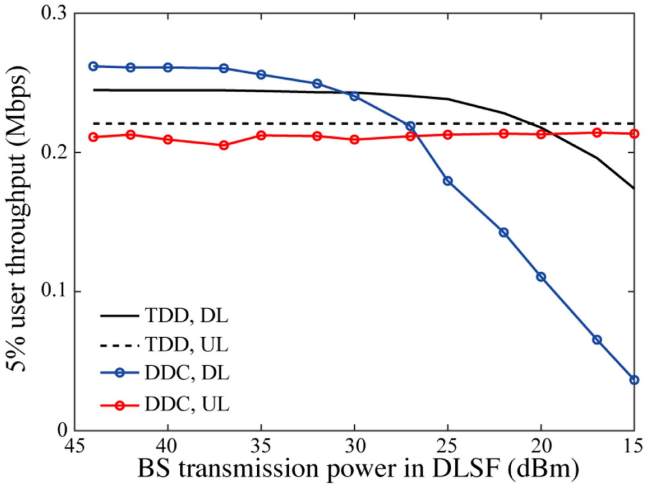

FIGURE 19. 5% user throughput as a function of BS transmission power in the DLSF when DDC is applied to both DLSF and ULSF.

2) EFFECT OF BS TRANSMISSION POWER

The IBFD application ratio as a function of $P_{\mathrm{BS}}^{\mathrm{ULSF}}$ is shown in Fig. 16. The IBFD application ratio increases as $P_{\mathrm{BS}}^{\mathrm{ULSF}}$ decreases when $P_{\mathrm{BS}}^{\mathrm{ULSF}} \geq -20$ dBm. However, the IBFD application ratio decreases as $P_{\mathrm{BS}}^{\mathrm{ULSF}}$ decreases when $P_{\mathrm{BS}}^{\mathrm{ULSF}} \leq -20$ dBm. This is because when $P_{\mathrm{BS}}^{\mathrm{ULSF}} \geq -20$ dBm, as $P_{\mathrm{BS}}^{\mathrm{ULSF}}$ decreases, the assumed UL-SINR, $\widehat{\gamma_{i,\,u_i}^{\mathrm{FD}}}$, shown in (18) is improved and the IBFD application condition is easily satisfied. However, when $P_{\mathrm{BS}}^{\mathrm{ULSF}} \leq -20$ dBm, the estimated SINR of DL, $\widehat{\gamma_{d_i,i}^{\mathrm{FD}}}$, shown in (19) deteriorates as $P_{\mathrm{BS}}^{\mathrm{ULSF}}$ decreases, and the number of DL-UEs that satisfy CQI ≥ 1 decreases.

The average user throughput as a function of $P_{\mathrm{BS}}^{\mathrm{ULSF}}$ is shown in Fig. 17. Unlike the IBFD application ratio, as $P_{\mathrm{BS}}^{\mathrm{ULSF}}$ decreases, the average DL user throughput decreases when $P_{\mathrm{BS}}^{\mathrm{ULSF}} \leq -10$ dBm. This is because when -20 dBm $\leq P_{\mathrm{BS}}^{\mathrm{ULSF}} \leq -10$ dBm, the impact of the degradation of the CQI of DL communications owing to the degradation of SINR of DL, $\widehat{\gamma_{d_i,i}^{\mathrm{FD}}}$, is smaller than the impact of increasing the IBFD application ratio. In particular, when $P_{\mathrm{BS}}^{\mathrm{ULSF}}$ is set to -5 dBm in the ULSF-DDC, it resulted in a 17.0% increase in the average DL user throughput compared with that of the TDD system, with only a 6.0% decrease in the average UL user throughput.

D. DDC

Finally, the performance of the DDC system when applied to both the DLSF and ULSF is evaluated by utilizing the parameters determined in the previous sections.

1) THROUGHPUT PERFORMANCE

The average and 5% user throughputs as functions of $P_{\mathrm{BS}}^{\mathrm{DLSF}}$ are shown in Figs. 18 and 19, respectively. Because $P_{\mathrm{BS}}^{\mathrm{ULSF}}$ is set to -5 dBm, the average user throughput and 5% DL user

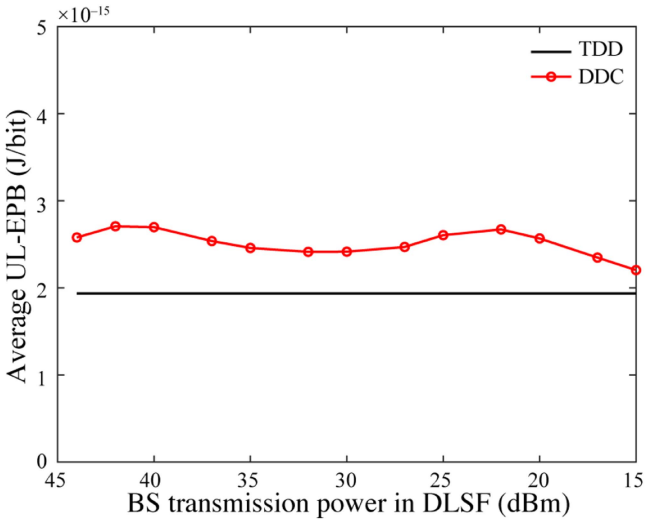

FIGURE 20. Average UL-EPB as a function of the BS transmission power in DLSF $P_{\mathrm{BS}}^{\mathrm{DLSF}}$ when DDC is applied to both the DLSF and ULSF.

throughputs are 16.1% and 7.0% higher, respectively, compared with those in the TDD system when $P_{\mathrm{BS}}^{\mathrm{DLSF}} = 44$ dBm. However, as $P_{\mathrm{BS}}^{\mathrm{DLSF}}$ decreases, the average DL and 5% user throughputs deteriorate because the IBFD application ratio in the DLSF increased and the SINR of DL, $\gamma_{d_i,i}^{\mathrm{FD}}$, shown in (4) decreases. In particular, when $P_{\mathrm{BS}}^{\mathrm{ULSF}} = -5$ dBm and $P_{\mathrm{BS}}^{\mathrm{DLSF}} = 32$ dBm, the average DL and UL user throughputs increase by 13.2% and 31.6%, respectively, compared with those in the TDD system, whereas the DL 5% user throughput increases by 2.5%, and the UL 5% user throughput degrades by 4.1%. Furthermore, with $P_{\mathrm{BS}}^{\mathrm{ULSF}} = -5$ dBm and $P_{\mathrm{BS}}^{\mathrm{DLSF}} = 27$ dBm, the average DL and UL user throughputs increase by 6.3% and 57.0%, respectively, compared with those in the TDD system, whereas the DL and UL 5% user throughputs decrease by 9.0% and 4.1%, respectively.

2) ENERGY PERFORMANCE

The average UL-EPB as a function of $P_{\mathrm{BS}}^{\mathrm{DLSF}}$ is shown in Fig. 20. Regardless of $P_{\mathrm{BS}}^{\mathrm{DLSF}}$, the average UL-EPB of the DDC system is lower than that of the TDD system. This is because the UL communications allocated to the DLSF required more power than the ULSF because of the SI, and interference from the BSs in other cells significantly degrades the quality of UL communications in the DLSF. However, this degradation resulted in an increase in the UL capacity by applying the DDC system. In particular, with $P_{\mathrm{BS}}^{\mathrm{DLSF}} = 32$ dBm, the average DL user throughput increases by 31.6%, whereas the average UL-EPB increases by 24.6%. Furthermore, when $P_{\mathrm{BS}}^{\mathrm{DLSF}} = 27$ dBm, the average DL user throughput increases by 57.0%, whereas the average UL-EPB increases by 27.5%.

V. CONCLUSION

This study proposed a DDC system in which FDC was achieved by introducing IBFD in a phased manner to a conventional static-TDD-based cellular system. We proposed and evaluated appropriate UE scheduling and transmission power control schemes for DDC systems in dense urban multi-cell environments. The proposed DDC system sufficiently suppressed ICI through a fully distributed resource allocation that did not require information exchange among neighboring cells. In particular, the propagation loss compensation factor α, the UE transmission power limit $P_{\mathrm{UE}}^{\mathrm{lim}}$, and the factor β related to the assumed UL-SINR calculation proved to be essential. By setting $\alpha = 0.4$ and $P_{\mathrm{UE}}^{\mathrm{lim}} = 9$ dBm for DLSF-DDC, and $\beta = 0.5$ for ULSF-DDC, the proposed DDC system improved the average throughput of DL by 13.2% and UL by 31.6% compared with the conventional TDD system, whereas the DL 5% user throughput also improved by 2.5%. The throughput improvement of the DL and UL users could be flexibly controlled by changing the main factors previously mentioned. The results of this study are expected to contribute to the realization of high-capacity wide-area IoT network backbone by improving the efficiency of utilization of limited spectral resources, especially in the Sub-6 GHz band. Although this paper focused on evaluating the basic architecture and fundamental characteristics of DDC systems, it is one of the future-works to evaluate or propose additional techniques for DDC systems when frequency-selective fading or multiple antennas are introduced. Another future issue is research on a simple method of parameter tuning for more realistic implementations.

REFERENCES

[1] Cisco, "Cisco annual internet report (2018–2023)," Mar. 2020. Accessed: Jul. 25, 2023. [Online]. Available: https://www.cisco.com/c/en/us/solutions/collateral/executive-perspectives/annual-internet-report/white-paper-c11-741490.html
[2] Y. Wang et al., "A primer on 3GPP narrowband Internet of Things," *IEEE Commun. Mag.*, vol. 55, no. 3, pp. 117–123, Mar. 2017.
[3] W. Yang et al., "Narrowband wireless access for low-power massive Internet of Things: A bandwidth perspective," *IEEE Wireless Commun.*, vol. 24, no. 3, pp. 138–145, Jun. 2017.
[4] X. Lin et al., "Positioning for the Internet of Things: A 3GPP perspective," *IEEE Commun. Mag.*, vol. 55, no. 12, pp. 179–185, Dec. 2017.
[5] H. Harada et al., "IEEE 802.15.4g based Wi-SUN communication systems," *IEICE Trans. Commun.*, vol. 100, no. 7, pp. 1032–1043, Jul. 2017.
[6] *IEEE Standard for Wireless Smart Utility Network Field Area Network (FAN)*, IEEE Standard 2857TM-2021, NJ, USA, Jun. 2021.
[7] T. Junjalearnvong, R. Okumura, K. Mizutani, and H. Harada, "Performance evaluation of multi-hop network configuration for Wi-SUN FAN systems," in *Proc. IEEE 16th Annun. Consum. Commun. Netw. Conf.*, 2019, pp. 1–6.
[8] Y. Xiang, R. Okumura, K. Mizutani, and H. Harada, "Data rate enhancement of FSK transmission scheme for IEEE 802.15.4-based field area network," *IEEE Sens. J.*, vol. 21, no. 7, pp. 9600–9611, Jan. 2021.
[9] S. Kadoi, H. Ochiai, R. Okumura, K. Mizutani, and H. Harada, "IEEE 802.15.4g/4x-based orthogonal frequency division multiplexing transmission scheme for wide area and mobile IoT communication systems," *IEEE Internet Things J*, vol. 9, no. 14, pp. 12673–12683, Dec. 2021.
[10] R. Hirakawa, R. Okumura, K. Mizutani, and H. Harada, "A novel routing method with load-balancing in Wi-SUN FAN network," in *Proc. IEEE World Forum Internet Things*, 2021, pp. 362–367.
[11] C. Ferreira et al., "A straightforward method to promote effective interoperability in Wi-SUN FAN smart grid networks," in *Proc. IEEE Latin-Amer. Conf. Commun.*, 2022, pp. 1–5.

[12] P. Yang, Y. Xiao, M. Xiao, and S. Li, "6G wireless communications: Vision and potential techniques," *IEEE Netw*, vol. 33, no. 4, pp. 70–75, Jul. 2019.
[13] M. Z. Chowdhury, M. Shahjalal, S. Ahmed, and Y. M. Jang, "6G wireless communication systems: Applications, requirements, technologies, challenges, and research directions," *IEEE Open J. Commun. Soc.*, vol. 1, pp. 957–975, Jul. 2020.
[14] T. Matsumura, H. Kuriki, K. Mizutani, and H. Harada, "Macro-cell capacity enhancement with dynamic full-duplex cellular system," in *Proc. 21st Int. Symp. Wireless Pers. Multimedia Commun.*, 2018, pp. 336–341.
[15] K. Nishikori, K. Terame, K. Mizutani, T. Matsumura, and H. Harada, "User throughput enhancement with dynamic full-duplex cellular system in dense urban multi-cell environment," in *Proc. IEEE 30th Annu. Int. Symp. Pers., Indoor Mobile Radio Commun.*, 2019, pp. 1–6.
[16] D. Bharadia, E. McMilin, and S. Katti, "Full duplex radios," in *Proc. ACM SIGCOMM Comput. Commun. Rev.*, 2013, pp. 375–386.
[17] D. Kim, H. Lee, and D. Hong, "A survey of in-band full-duplex transmission: From the perspective of PHY and MAC layers," *IEEE Commun. Surv. Tut.*, vol. 17, no. 4, pp. 2017–2046, Feb. 2015.
[18] A. Sabharwal, P. Schniter, D. Guo, D. W. Bliss, S. Rangarajan, and R. Wichman, "In-band full-duplex wireless: Challenges and opportunities," *IEEE J. Sel. Areas Commun.*, vol. 32, no. 9, pp. 1637–1652, Sep. 2014.
[19] K. Mizutani and H. Harada, "Quantization noise reduction by digital signal processing-assisted analog-to-digital converter for in-band full-duplex systems," *IEEE Trans. Wireless Commun.*, vol. 21, no. 8, pp. 6643–6655, Aug. 2022.
[20] M. Amjad, F. Akhtar, M. H. Rehmani, M. Reisslein, and T. Umer, "Full-duplex communication in cognitive radio networks: A survey," *IEEE Commun. Surv. Tut.*, vol. 19, no. 4, pp. 2158–2191, Jun. 2017.
[21] M. Tilan, H. Ayar, H. Nawaz, O. Gurbuz, and I. Tekin, "Monostatic antenna in-band full duplex radio: Performance limits and characterization," *IEEE Trans. Veh. Technol.*, vol. 68, no. 5, pp. 4786–4799, Mar. 2019.
[22] K. Fukushima, S. Mori, K. Mizutani, and H. Harada, "Throughput enhancement of dynamic full-duplex cellular system by distributing base station reception function," *IEEE Open J. Veh. Technol.*, vol. 4, pp. 114–126, Dec. 2022.
[23] J. Zhou et al., "Integrated full duplex radios," *IEEE Commun. Mag.*, vol. 55, no. 4, pp. 142–151, Apr. 2017.
[24] D. Korpi et al., "Full-duplex mobile device: Pushing the limits," *IEEE Commun. Mag.*, vol. 54, no. 9, pp. 80–87, Sep. 2016.
[25] A. Ershadi and K. Entesari, "A 0.5-to-3.5 GHz self-interference-canceling receiver for in-band full-duplex wireless," in *Proc. IEEE Radio Freq. Integ. Circ. Symp.*, 2019, pp. 151–154.
[26] S. Khaledian, F. Farzami, B. Smida, and D. Erricolo, "Inherent self-interference cancellation for in-band full-duplex single antenna systems," *IEEE Trans. Microw. Theory Techn.*, vol. 66, no. 6, pp. 2842–2850, Jun. 2018.
[27] T. Matsumura, "On the analog self-interference cancellation for in-band full-duplex radio with compensation for inherent frequency response," in *Proc. IEEE 24st Int. Symp. Wireless Pers. Multimedia Commun.*, 2021, pp. 1–6.
[28] M. Emara, P. Rosson, K. Roth, and D. Dassonville, "A full duplex transceiver with reduced hardware complexity," in *Proc. IEEE Glob. Telecommun. Conf.*, 2017, pp. 1–6.
[29] E. Ahmed and A. M. Eltawil, "All-digital self-interference cancellation technique for full-duplex systems," *IEEE Trans. Wireless Commun.*, vol. 14, no. 7, pp. 3519–3532, Jul. 2015.
[30] S. Liu, K. Mizutani, T. Matsumura, and H. Harada, "Self-interference cancellation utilizing superposition modulation technique for single carrier full-duplex system," in *Proc. IEEE 91st Veh. Technol. Conf.*, 2020, pp. 1–6.
[31] H. Vogt, G. Enzner, and A. Sezgin, "State-space adaptive nonlinear self-interference cancellation for full-duplex communication," *IEEE Trans. Signal Process.*, vol. 67, no. 11, pp. 2810–2825, Apr. 2019.
[32] S. Mori, K. Mizutani, and H. Harada, "A digital self-interference cancellation scheme for in-band full-duplex-applied 5G system and its software-defined radio implementation," *IEEE Open J. Veh. Technol.*, vol. 4, pp. 444–456, May 2023.
[33] H. Guo, S. Wu, H. Wang, and M. Daneshmand, "DSIC: Deep learning based self-interference cancellation for in-band full duplex wireless," in *Proc. IEEE Glob. Telecommun. Conf.*, 2019, pp. 1–6.
[34] M. S. Sim, M. Chung, D. Kim, J. Chung, D. K. Kim, and C.-B. Chae, "Nonlinear self-interference cancellation for full-duplex radios: From link-level and system-level performance perspectives," *IEEE Commun. Mag.*, vol. 55, no. 9, pp. 158–167, Sep. 2017.
[35] S. Mori, K. Mizutani, and H. Harada, "In-band full-duplex-applicable area expansion by inter-user interference reduction using successive interference cancellation," *IEICE Trans. Commun.*, V vol. 105, no. 2, pp. 168–176, Feb. 2022.
[36] G. C. Alexandropoulos, M. Kountouris, and I. Atzeni, "User scheduling and optimal power allocation for full-duplex cellular networks," in *Proc. IEEE 17th Int. Workshop Sig. Process Adv. Wireless Commun.*, Jul. 2016, pp. 1–6.
[37] Z. Liu, Y. Liu, and F. Liu, "Joint resource scheduling for full-duplex cellular system," in *Proc. IEEE 22nd Inter. Conf. Telecommun.*, Apr. 2015, pp. 85–90.
[38] H. Fawaz, S. Lahoud, M. E. Helou, and M. Ibrahim, "Max-SINR scheduling in full-duplex OFDMA cellular networks with dynamic arrivals," in *Proc. IEEE Symp. Comp. Commun.*, Jul. 2017, pp. 1–6.
[39] X. Shen, X. Cheng, L. Yang, M. Ma, and B. Jiao, "On the design of the scheduling algorithm for the dull duplexing wireless cellular network," in *Proc. IEEE Glob. Commun. Conf.*, Dec. 2013, pp. 4970–4975.
[40] L. Xue, Y. Cheng, Y. Zhou, and B. Qu, "Next generation TDD cellular communication," in *Proc. IEEE Asilomar Conf. Signals Syst. Comput.*, Nov. 2015, pp. 1036–1040.
[41] J. Liu, R. Fan, H. Wang, J. Liu, and F. Wang, "Dynamic TDD testbed and field measurements," in *Proc. IEEE 83rd Veh. Technol. Conf.*, 2016, pp. 1–5.
[42] Z. Shen, A. Khoryaev, E. Eriksson, and X. Pan, "Dynamic uplink downlink configuration and interference management in TD-LTE," *IEEE Commun. Mag.*, vol. 50, no. 11, pp. 51–59, Nov. 2012.
[43] *Evolved Universal Terrestrial Radio Access (E-UTRA); Physical Layer Procedures (Release 15)*, 3GPP, Sophia Antipolis, France, Tech. Specification 36.213, v.15.7.0, Sep. 2019.
[44] *Study on 3D Channel Model for LTE (Release 12)*, 3GPP, Sophia Antipolis, France, Tech. Specification 36.873, v.12.7.0, Jan. 2018.
[45] *Evolved Universal Terrestrial Radio Access (E-UTRA); Physical Channels and Modulation (Release 15)*, 3GPP, Sophia Antipolis, France, Tech. Specification 36.211, v.15.7.0, 3GPP, Sep. 2019.
[46] *Study on LTE Device to Device Proximity Services; Radio Aspects (Release 12)*, 3GPP, Sophia Antipolis, France, Tech. Specification 36.843, v.12.0.1, Mar. 2014.
[47] M. Duarte and A. Sabharwal, "Full-duplex wireless communications using off-the-shelf radios: Feasibility and first results," in *Proc. IEEE Asilomar Conf. Signals, Syst. Comput.*, pp. 1558–1562, Nov. 2010.

KEIICHI MIZUTANI (Member, IEEE) received the B.E. degree in engineering from Osaka Prefecture University, Sakai, Japan, in 2007, and the M.E. and Ph.D. degrees in engineering from the Tokyo Institute of Technology, Tokyo, Japan, in 2009 and 2012, respectively. In 2010, he was an invited Researcher with Fraunhofer Heinrich Hertz Institute, Berlin, Germany. From 2012 to 2014, he was a Researcher with the National Institute of Information and Communications Technology (NICT), Tokyo, Japan. From 2014 to 2021, he was an Assistant Professor with the Graduate School of Informatics, Kyoto University, Kyoto, Japan. From 2021 to 2022, he was an Associate Professor with the Kyoto University School of Platforms (KUSP). He is currently an Associate Professor with the Graduate School of Informatics, Kyoto University. His current research interests include physical layer technologies in white space communications, dynamic spectrum access, wireless smart utility networks (Wi-SUN), and 4G/5G/6G systems, including OFDM, OFDMA, MIMO, multi-hop relay network, and full-duplex cellular systems. Since joining NICT, he has been involved in IEEE 802 standardization activities, namely 802.11af, 802.15.4m, and 802.22b. He was the recipient of the Special Technical Awards from IEICE SR Technical Committee in 2009 and 2017, Best Paper Award from IEICE SR Technical Committee in 2010 and 2020, Young Researcher's Award from IEICE SRW Technical Committee in 2016, Best Paper Award from WPMC2017, WPMC2020, and WPMC2022, and the Best Paper Presentation Award (1st Place) from IEEE WF-IoT 2020.

KAZUKI NISHIKORI received the B.E. degree from the Faculty of Engineering, Kyoto University, Kyoto, Japan, in 2019, and the M.I. degree from the Graduate School of Informatics, Kyoto University, in 2021.

KYOYA TERAMAE received the B.E. degree from the Faculty of Engineering, Kyoto University, Kyoto, Japan, in 2018, and the M.I. degree from the Graduate School of Informatics, Kyoto University, in 2020. He was the recipient of the Young Researcher's Encouragement Award from IEEE VTS Tokyo Chapter in 2019.

HIROTO KURIKI received the B.E. degree from the Faculty of Engineering, Kyoto University, Kyoto, Japan, in 2016, and the M.I. degree from the Graduate School of Informatics, Kyoto University, in 2018. He was the recipient of the Young Researcher's Encouragement Award from IEEE VTS Tokyo Chapter in 2017 and Student Award from IEICE SRW Technical Committee in 2018.

TAKESHI MATSUMURA (Member, IEEE) received the M.S. degree in electronics engineering and the Ph.D. degree in nano-mechanics engineering from Tohoku University, Sendai, Japan, in 1998 and 2010, respectively. He was an Associate Professor with Kyoto University. During 1998–2007, he was engaged in the R&D of wireless communications devices with some companies. In April 2007, he joined the National Institute of Information and Communications Technology (NICT), as a Researcher and was engaged in whitespace communication systems, and 5G mobile communication systems. During 2016–2019, he was engaged in baseband signal processing, whitespace communication systems, and 5G as an Associate Professor with Kyoto University. He is currently the Director of NICT, and a researcher with Kyoto University. His research interests include white-space communication systems, wide-area wireless network systems, and 5G and beyond 5G mobile communication systems.

HIROSHI HARADA (Senior Member, IEEE) is currently a Professor with the Graduate School of Informatics, Kyoto University, Kyoto, Japan, and an Executive Research Director of Wireless Networks Research Center, National Institute of Information and Communications Technology (NICT), Tokyo, Japan. In 1995, he joined the Communications Research Laboratory, Ministry of Posts and Communications (currently NICT). Since 1995, he has researched software radio, cognitive radio, dynamic spectrum access network, wireless smart ubiquitous network (Wi-SUN), and broadband wireless access systems. He also has joined many standardization committees and forums in the United States and in Japan and fulfilled important roles for them, especially IEEE 1900 and IEEE 802. He was the Chair of IEEE DySpan Standards Committee and Vice Chair of IEEE 802.15.4g, IEEE 802.15.4m, IEEE 1900.4, and TIA TR-51. He was a Board of Directors of IEEE Communication Society Standards Board, SDR forum, DSA alliance, and WhiteSpace alliance. He is a Co-Founder of Wi-SUN alliance and was the Chairman of the Board during 2012–2019 and as of 2024. He is also involved in many other activities related to telecommunications. He has authored the book titled *Simulation and Software Radio for Mobile Communications* (Artech House, 2002). He is the Vice Chair of IEEE 2857, IEEE 802.15.4aa, and IEEE 802.15.4ad. He was the Chair of the IEICE Technical Committee on Software Radio (TCSR) and Chair of Public Broadband Mobile Communication Development Committee, ARIB. He was the recipient of the achievement awards in 2006 and 2018 and Fellow of IEICE in 2009, and achievement awards of ARIB in 2009, 2018, and 2022, respectively, on the topic of research and development on software radio, cognitive radio, and Wi-SUN.